

Anisotropy-controlled topological stability of discrete vortex solitons in optically induced photonic lattices

Bernd Terhalle,^{1,*} Dennis Göries,¹ Tobias Richter,² Patrick Rose,¹ Anton S. Desyatnikov,³ Friedemann Kaiser,² and Cornelia Denz¹

¹Institut für Angewandte Physik and Center for Nonlinear Science (CeNoS), Westfälische Wilhelms-Universität, 48149 Münster, Germany

²Institut für Angewandte Physik, Technische Universität Darmstadt, 64289 Darmstadt, Germany

³Nonlinear Physics Centre, Research School of Physics and Engineering, The Australian National University, Canberra, Australian Capital Territory 0200, Australia

*Corresponding author: bernd.terhalle@uni-muenster.de

Received October 29, 2009; revised December 15, 2009; accepted December 16, 2009;
posted January 8, 2010 (Doc. ID 119173); published February 12, 2010

We realize an experimental control over the topological stability of three-lobe discrete vortex solitons by modifying the symmetry of a hexagonal photonic lattice optically induced in a photorefractive crystal. By continuously deforming the lattice wave in one transverse direction, we manipulate the coupling between lattice sites and induce or inhibit the reversal of soliton vorticity. © 2010 Optical Society of America
OCIS codes: 190.4420, 190.5530.

Optically induced photonic lattices provide an access to the rich physical phenomena of linear and self-trapped waves in periodic potentials [1]. Among diverse types of nonlinear lattice excitations [2,3] the discrete vortex solitons [4,5] attract particular attention owing to their feature of localized persistent currents around phase singularities [6]. Stable four-lobe vortices were experimentally generated in square lattices [7,8], whereas six-lobe vortices [9] as well as multivortex structures [10] have been studied in hexagonal lattices. The reversal of the vortex current, suggested for asymmetric vortices [11], and complex topological transformations involving several dislocations [12–14] are possible because of the broken rotational symmetry of the periodic medium. Similarly, the topological stability of lattice vortex solitons, i.e., the stability of phase and power flow, crucially depends on the lattice symmetry, and it is strongly affected by the orientation anisotropy of the photorefractive nonlinearity [9,10,15].

The simplest lowest-order discrete vortex soliton with only three intensity lobes and a unit topological charge in hexagonal lattices is a very robust entity in isotropic saturable media [16]. At the same time, the symmetry of the refractive index pattern optically induced in a photorefractive crystal significantly depends on the level of saturation as well as the transverse orientation of the periodic lattice wave [17]. Therefore, the spatial phase structure of a three-lobe vortex needs to be deformed, similar to asymmetric discrete vortex solitons in isotropic media [11]. It follows that the interplay between the asymmetry of a vortex and the orientation anisotropy of the lattice provides an *additional degree of freedom* in building stable vortex solitons.

In this Letter, we employ the anisotropy of optically induced hexagonal lattices to control the topological stability of single-charge three-lobe discrete vortex solitons. We demonstrate that the *continuous* transverse deformation of the lattice wave, preserv-

ing its nondiffracting propagation, allows tailoring the coupling between lattice sites. As a result, the switching between topologically unstable and stable solitons is demonstrated experimentally.

We begin by constructing the nondiffracting hexagonal lattice wave $U(\mathbf{r}, z)$ as an interference of three plane waves, $U = U_0 \sum_{j=1}^3 \exp(i\mathbf{k}_j \mathbf{r} + ik_z z)$, with equal amplitudes U_0 and the transverse wavevectors \mathbf{k}_j laying on a circle, $|\mathbf{k}_j| = k$ so that $k^2 + k_z^2 = k_0^2$. Here, $k_0 = 2\pi n_0 / \lambda$ is the wavevector, n_0 is the medium refractive index, and λ is the wavelength. The lattice period in the y -direction is $d_y = \eta d_x$ with a variable η . For the horizontal orientation of hexagons we choose $\mathbf{k}_1 = \{-k, 0\}$ so that $\mathbf{k}_{2,3} = \{\sqrt{k^2 - k_y^2}, \pm k_y\}$, with the parameter $k_y = 2\pi / \eta d_x$. The intensity of the lattice wave with the amplitude $I_0 = \max I$ is given by

$$I = \frac{I_0}{3} \left[1 + \frac{2}{3} \cos\left(\frac{4\pi y}{d_x \eta}\right) + \frac{4}{3} \cos\left(\frac{2\pi y}{d_x \eta}\right) \cos\left(\frac{2\pi x}{d_x}\right) \right]. \quad (1)$$

The hexagonal lattice wave is symmetric for $\eta = \sqrt{3}$, “squeezed” in the y -direction for $\eta < \sqrt{3}$, and “stretched” for $\eta > \sqrt{3}$.

In numerical simulations, we use the anisotropic model of photorefractive nonlinearity [9,10,15], with parameters close to experimental conditions. Since we consider discrete vortex solitons in the semi-infinite gap, we assume that the lobes of a vortex are centered on the lattice sites and only weakly coupled. Thus, we adopt the model of [11], with the vortex soliton field, $E = \sum_{j=1}^3 \psi(\mathbf{r}_j) \exp(i\phi_j + i\beta z)$, given by the superposition of fundamental discrete solitons with real envelopes $\psi(\mathbf{r})$ and soliton constant β . In this approach, the vortex lobes are positioned at the neighboring lattice sites, $\mathbf{r}_1 = \{0, 0\}$, $\mathbf{r}_2 = \{d_x, 0\}$, and $\mathbf{r}_3 = \{d_x/2, \eta d_x/2\}$, and each lobe has a distinct phase ϕ_j . The initial phase difference between two lobes is

$|\phi_i - \phi_j| = 2\pi/3 \quad \forall i, j; i \neq j$. To create a stable vortex soliton, the balance of the power flow between the lobes is required, $\sum_{j=1}^3 c_{jn} \sin(\phi_j - \phi_n) = 0$ (for each lobe $n=1, 2, 3$), where the integral coupling coefficients $c_{jn} = c_{nj}$ depend on the nonlinearity, the soliton $\psi(\mathbf{r})$, and the lattice $I(\mathbf{r})$ [11].

In contrast to the isotropic model [16], the refractive index pattern optically induced by the symmetric hexagonal wave ($\eta = \sqrt{3}$) displays clear anisotropic features [see Fig. 1(a)]. In particular, while in the horizontal x -direction the lattice sites are separated by (dark) repulsive potentials, in the “diagonal” directions the modulation contrast between neighboring sites is much lower. As a result, the coupling between sites in the x -direction is diminished in comparison with the diagonal coupling, $c_{12} \ll c_{23}$ (and $c_{13} \equiv c_{23}$ from symmetry considerations). The discrete diffraction pattern in Fig. 1(b) reflects this anisotropy, and it is influenced by the vorticity of the input state with a positive unit topological charge and a counterclockwise power flow.

In the nonlinear regime the diffraction is suppressed, and a localized self-trapped discrete vortex is observed at the output in Fig. 1(c). However, because of the asymmetric coupling between lattice sites the power flows between the individual vortex lobes are no longer balanced and lead to continuous phase changes. The actual dynamics involves topological reactions between several phase dislocations [14], and it results in the inversion of the vortex current [see the clockwise arrow in Fig. 1(d)]. While in isotropic square lattices the flipping of the topological charge of asymmetric vortices is triggered by an external perturbation [11,18], here it arises due to the intrinsic anisotropy of the photorefractive response.

The key to stabilize vortices is to restore the coupling symmetry by the deformation of the lattice wave equation (1). Keeping the period d_x as a constraint largely preserves the coupling c_{12} in the x -direction. Therefore, the lattice has to be stretched, $\eta > \sqrt{3}$, to reduce coefficients c_{23} and c_{13} . The actual necessary amount of stretching depends on particular parameters of the lattice (I_0 and d_x) as well as the

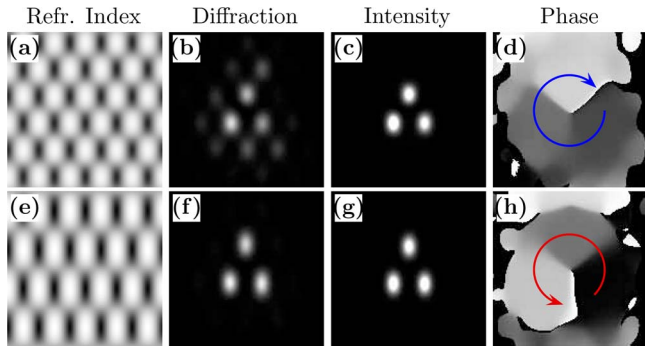


Fig. 1. (Color online) Comparison between symmetric [(a)–(d), $\eta = \sqrt{3}$] and stretched [(e)–(h), $\eta = 2.5$] lattices: (a), (e) refractive index; (b), (f) output intensity in the linear regime of discrete diffraction; (c), (g) output intensity and (d), (h) phase profiles of discrete vortex solitons (propagation distance of $z = 33$ mm). The arrows in (d) and (h) show the direction of current.

soliton envelope ψ . For our choice of parameters the optimal value is found to be $\eta = 2.5$. The corresponding refractive index pattern is shown in Fig. 1(e).

The reduction in coupling coefficients by stretching suppresses tunneling between sites and the discrete diffraction is significantly reduced [cf. Figs. 1(b) and 1(f)]. At the same time, the power flow between vortex lobes is symmetric and, in the nonlinear regime, the discrete vortex soliton preserves its topological charge [see the counterclockwise arrow in Fig. 1(h)].

To test our theoretical predictions in experiment, we employ a setup similar to the one described in [9] using two programmable spatial light modulators to generate the lattice wave and the probe beam input. All experiments are performed in a 20 mm long photorefractive Ce-doped strontium barium niobate crystal, which is externally biased with a direct current electric field of approximately 2 kV/cm directed along its optical c -axis.

First, we consider the propagation of a three-lobe vortex soliton with a unit topological charge in a hexagonal lattice induced by the symmetric lattice wave

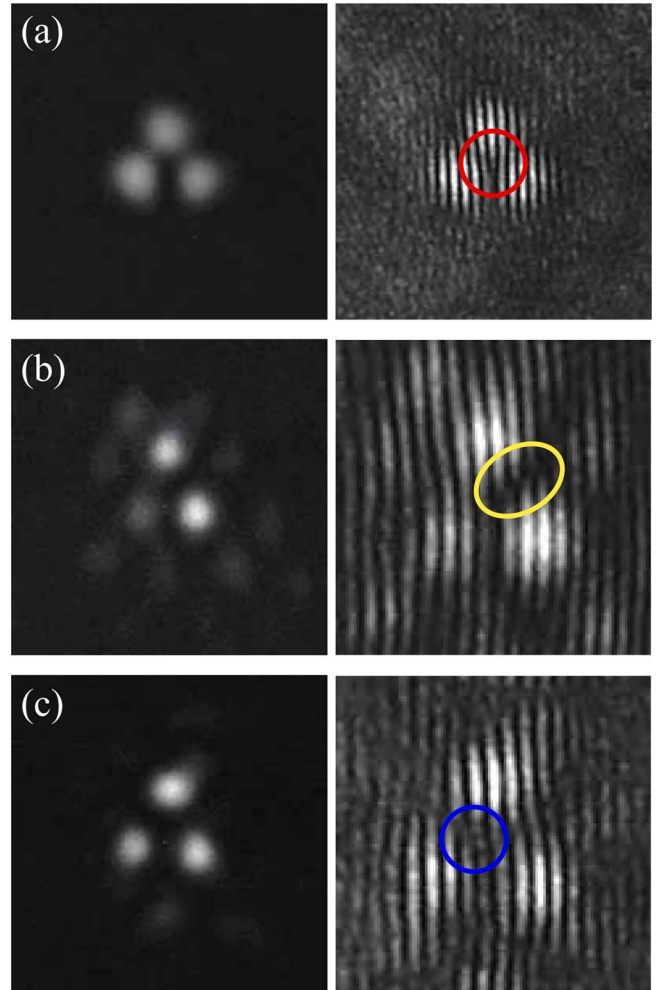


Fig. 2. (Color online) Experimental results for symmetric hexagonal lattice wave. Intensity (left panels) and interferograms (right panels) are shown for (a) the input vortex beam of unit charge (fork up, red circle), (b) discrete diffraction output with zero charge (two opposite dislocations, yellow oval), and (c) the nonlinear output with flipped charge (fork down, blue circle).

with a horizontal lattice constant of $d_x \approx 30 \mu\text{m}$. Figure 2(a) shows the corresponding intensity and phase profiles of the input beam. The latter is revealed by the interferogram with the fork-type vortex dislocation. At low input power ($\approx 20 \text{ nW}$), the output shows discrete diffraction and the phase profile gets distorted. More careful examination reveals that the number of vertical interference fringes coming in and out of the yellow oval in Fig. 2(b) is the same. Therefore, inside the triangle between three major intensity peaks (initially excited sites), there are two dislocations of the opposite charge so that the total topological charge is zero. Furthermore, with the increase in power to $\approx 150 \text{ nW}$, we observe in Fig. 2(c) three well-defined intensity spots closely resembling the input structure, but the phase profile now shows the opposite topological charge. Thus, in full agreement with our simulations in Figs. 1(c) and 1(d), alongside with nonlinear localization of intensity, we observe the reversal of the vortex current.

The experimental results for the stretched lattice with $d_y/d_x=2.5$ are depicted in Fig. 3 [cf. Figs. 1(e)–1(h)]. The diffraction in the low power regime is much less pronounced than in the symmetric case and it is hardly visible in Fig. 3(b). However, the most

important result here is that the phase profile is preserved even in the nonlinear output in Fig. 3(c). Since all the other parameters have been chosen to be the same as in the unstretched lattice in Fig. 2, the clear differences in phase profiles can be fully attributed to the stretching of the lattice and the resulting symmetric coupling. Thus, our experiments clearly prove the possibility to control the charge flip in anisotropic hexagonal photonic lattices by stretching the lattice along its vertical direction.

In conclusion, we introduce an anisotropic manipulation of the symmetry of an optically induced photonic lattice as an additional tool to tune its waveguiding properties. We demonstrate that, using elementary three-lobe discrete vortices in hexagonal lattices, simple one-dimensional deformation of the lattice wave allows one to adjust the coupling between lattice sites and to control the power flow between excited waveguides.

References

1. J. W. Fleischer, M. Segev, N. K. Efremidis, and D. N. Christodoulides, *Nature* **422**, 147 (2003).
2. F. Lederer, G. I. Stegeman, D. N. Christodoulides, G. Assanto, M. Segev, and Y. Silberberg, *Phys. Rep.* **463**, 1 (2008).
3. Y. V. Kartashov, V. A. Vysloukh, and L. Torner, *Prog. Opt.* **52**, 63 (2009).
4. P. G. Kevrekidis, B. A. Malomed, and Yu. B. Gaididei, *Phys. Rev. E* **66**, 016609 (2002).
5. J. Yang and Z. H. Musslimani, *Opt. Lett.* **28**, 2094 (2003).
6. A. S. Desyatnikov, Yu. S. Kivshar, and L. Torner, *Prog. Opt.* **47**, 291 (2005).
7. D. N. Neshev, T. J. Alexander, E. A. Ostrovskaya, Yu. S. Kivshar, H. Martin, I. Makasyuk, and Z. Chen, *Phys. Rev. Lett.* **92**, 123903 (2004).
8. J. W. Fleischer, G. Bartal, O. Cohen, O. Manela, M. Segev, J. Hudock, and D. N. Christodoulides, *Phys. Rev. Lett.* **92**, 123904 (2004).
9. B. Terhalle, T. Richter, K. J. H. Law, D. Göries, P. Rose, T. J. Alexander, P. G. Kevrekidis, A. S. Desyatnikov, W. Krolikowski, F. Kaiser, C. Denz, and Yu. S. Kivshar, *Phys. Rev. A* **79**, 043821 (2009).
10. B. Terhalle, T. Richter, A. S. Desyatnikov, D. N. Neshev, W. Krolikowski, F. Kaiser, C. Denz, and Yu. S. Kivshar, *Phys. Rev. Lett.* **101**, 013903 (2008).
11. T. J. Alexander, A. A. Sukhorukov, and Yu. S. Kivshar, *Phys. Rev. Lett.* **93**, 063901 (2004).
12. A. Ferrando, M. Zacares, M. A. Garcia-March, J. A. Monsoriu, and P. F. de Cordoba, *Phys. Rev. Lett.* **95**, 123901 (2005).
13. A. Bezryadina, E. Eugenieva, and Z. Chen, *Opt. Lett.* **31**, 2456 (2006).
14. A. Bezryadina, D. N. Neshev, A. S. Desyatnikov, J. Young, Z. Chen, and Yu. S. Kivshar, *Opt. Express* **14**, 8317 (2006).
15. T. Richter and F. Kaiser, *Phys. Rev. A* **76**, 033818 (2007).
16. T. J. Alexander, A. S. Desyatnikov, and Yu. S. Kivshar, *Opt. Lett.* **32**, 1293 (2007).
17. A. S. Desyatnikov, N. Sagemerten, R. Fischer, B. Terhalle, D. Träger, D. N. Neshev, A. Dreischuh, C. Denz, W. Krolikowski, and Yu. S. Kivshar, *Opt. Express* **14**, 2851 (2006).
18. M. I. Rodas-Verde, H. Michinel, and Yu. S. Kivshar, *Opt. Lett.* **31**, 607 (2006).

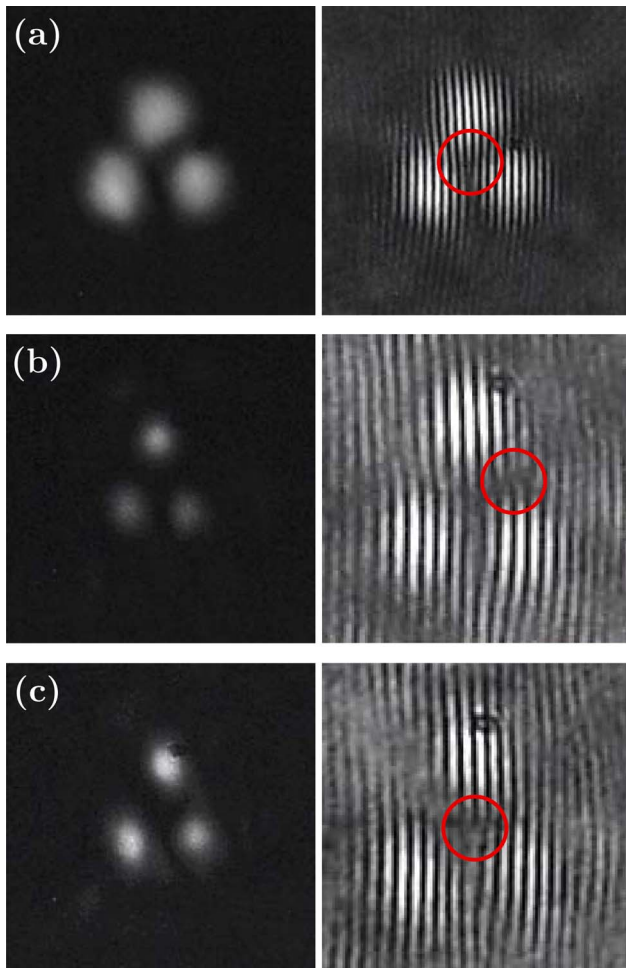


Fig. 3. (Color online) Experimental results for stretched hexagonal lattice wave; notations are similar to Fig. 2. Note the same topological charge (fork up, red circle) in all interferograms.